Journal of
Synchrotron Radiation

ISSN 0909-0495

Received 7 August 2010
Accepted 20 December 2010

Feasibility of in-line instruments for high-resolution inelastic X-ray scattering

W. Sturhahn* and T. S. Toellner

Advanced Photon Source, Argonne National Laboratory, 9700 South Cass Avenue, Argonne, IL 60439, USA. E-mail: wolfgang.sturhahn@jpl.nasa.gov

Inelastic X-ray scattering instruments in operation at third-generation synchrotron radiation facilities are based on backreflections from perfect silicon crystals. This concept reaches back to the very beginnings of high-energy-resolution X-ray spectroscopy and has several advantages but also some inherent drawbacks. In this paper an alternate path is investigated using a different concept, the 'M^4 instrument'. It consists of a combination of two in-line high-resolution monochromators, focusing mirrors and collimating mirrors. Design choices and performance estimates in comparison with existing conventional inelastic X-ray scattering instruments are presented.

Keywords: X-ray optics; inelastic X-ray scattering.

1. Introduction

Inelastic X-ray scattering (IXS) with energy resolution at the meV level has developed into a valuable investigative tool over the last decade (Burkel, 2000; Krisch & Sette, 2007). The high brilliance of third-generation synchrotron radiation sources in combination with refined manufacturing methods for spherically bent backscattering analyzers form the base for present-day meV-resolution IXS instruments. Backreflections or near-backreflections have the advantage of combining meV-level energy resolution with mrad-level angular acceptance. This unique situation allowed IXS instruments to be designed and built that provide sufficient counting rates in experiments of a variety of scientific areas. Even though the use of backreflections has been very successful, we also experienced certain disadvantages. In particular, the energy of operation and the energy resolution of the IXS instrument are determined by the choice of analyzer material which has traditionally been silicon or germanium. Studies have therefore investigated the use of materials such as sapphire (Yavas *et al.*, 2007) or quartz (Sutter *et al.*, 2006) instead, but the poorer crystal quality of such materials has so far prevented their use in high-resolution instruments. Bortel *et al.* (2000) realised the possibility of replacing the spherically bent backscattering analyzer with a high-resolution monochromator using two flat asymmetrically cut silicon crystals. Their device provided an energy resolution of 89 meV at an operating energy of 8.979 keV. However, the angular acceptance of their device was not sufficient to function as a practical IXS instrument, *i.e.* the inelastically scattered intensity was too low for applications to scientific problems. Later the addition of collimating mirrors was suggested as a means of obtaining much larger angular acceptances even at energy bandwidths below 1 meV (Shvydko, 2004).

In this paper we explore how the addition of achromatic focusing and collimating elements could improve the design of Bortel *et al.* (2000) and produce a practical IXS instrument as envisioned earlier (Shvydko, 2004). We will call this concept the 'M^4 instrument' (derived from the monochromator–mirror–mirror–monochromator arrangement), which is illustrated schematically in Fig. 1. It has several critical components: an in-line high-resolution monochromator to reduce the X-ray bandwidth on the sample; focusing mirrors to reduce the size of the X-ray beam at the sample position; collimating mirrors to collect inelastically scattered X-rays from a reasonably large solid angle; an in-line high-resolution monochromator to spectrally filter (analyze) the inelastically scattered X-rays. Monochromators with high efficiencies that produce energy bandwidths in the meV regime have been developed and tested for many years and are part of day-

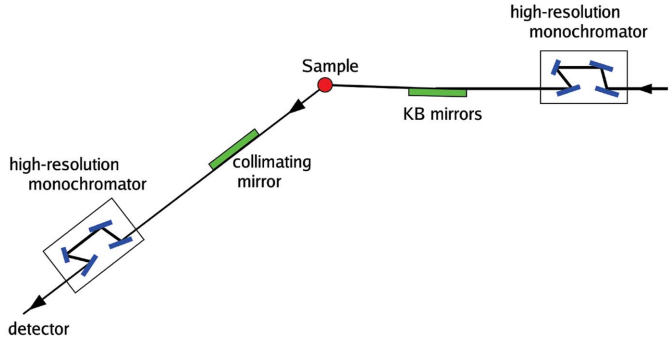

Figure 1
Schematic of the M^4 instrument. A high-resolution monochromator is followed by focusing mirrors. The inelastically scattered radiation is collimated before being analyzed by a second high-resolution monochromator. The scattering planes for monochromators and inelastic scattering need not be the same.

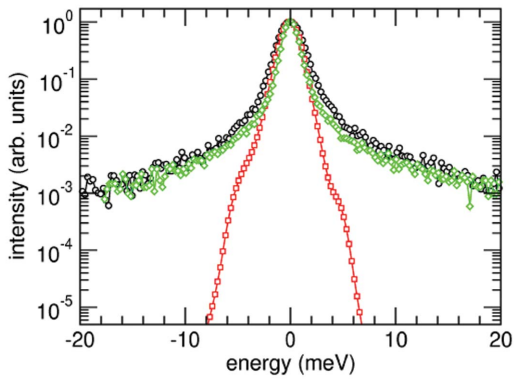

Figure 2
Comparison of resolution functions. Black circles: APS 3-ID, 2.2 meV FWHM, 21.6 keV. Green diamonds: APS 30-ID, 1.5 meV FWHM, 23.7 keV. Both instruments feature backreflection analyzers. Red squares: M^4 instrument calculated as a self-convolution of the measured resolution function of the in-line monochromator operating at APS 3-ID, 1.6 meV FWHM, 14.4 keV. The 'bumps' result from the specific combination of asymmetric Bragg reflections of different order.

to-day operations in several beamlines at third-generation synchrotron radiation facilities. The monochromators are mainly used for nuclear resonant scattering experiments (Mooney *et al.*, 1994; Chumakov *et al.*, 1996; Toellner *et al.*, 1997, 2001, 2006*b*; Hu *et al.*, 1999; Toellner, 2000; Chumakov *et al.*, 2000; Baron *et al.*, 2001; Yabashi *et al.*, 2001; Zhao *et al.*, 2002) but are also part of momentum-resolved IXS instruments at the Advanced Photon Source (Sinn *et al.*, 2001; Toellner *et al.*, 2006*a*).

The M^4 instrument has major advantages over existing IXS instruments based on backreflection analyzers: the operating energy is not tied to specific backreflection energies; the energy resolution is virtually independent of the operating energy, *i.e.* the same M^4 instrument may provide resolutions between 1 meV and 1 eV; the shape of the resolution function is devoid of the extended wings found in backreflection-based IXS instruments. The latter point is illustrated in Fig. 2. The M^4 instrument shows an almost complete suppression of wings which is a result of the four-reflection design of the monochromators. This property is not significantly influenced by the energy resolution. The sample area in the M^4 instrument is mostly unobstructed by detector assemblies, but, as we will see later, for large angular acceptances the collimating mirror has to be close to the sample and may somewhat encroach on the sample area.

The critical task in the design of an M^4 instrument is the optimization of the overall efficiency. In particular, the capacity of the collimation mirror to reduce angular divergence and thus a large angular acceptance of the analyzer is most important. The design of the collimating mirror in combination with the analyzing monochromator presents challenges that will be described in the following.

2. Collimating mirror

The purpose of the collimating mirrors is to adapt the angular divergence of the inelastically scattered X-rays to the angular acceptance of the analyzing monochromator. Practical designs for analyzing monochromators with operating energies of 9–15 keV achieve about 10–100 µrad angular acceptance in the scattering plane. A lower operating energy typically permits higher angular acceptances.

The collimation of X-rays by a mirror with a curved surface has two important contributions of different origin. On one hand the collimation of a divergent point source is governed by the exact shape of the reflecting mirror surface. On the other hand the spatial extent of the divergent source limits the best possible collimation and results in a lowest possible divergence of the collimated X-rays. The source size contribution is independent of the mirror surface shape but grows with increasing source size and decreasing distance between mirror and source.

2.1. Mirror shape

Assume a flat mirror that has reflecting length L, is operated at an angle of incidence θ, and its proximal edge is positioned at a distance d from the sample center. If the ratio d/L is reasonably large, say larger than 1, then the height of the reflected beam is estimated by $h = \theta L$, and the angular acceptance is $\delta\theta = 2\theta h/(2d\theta + h)$. For a given beam height h, a large angular acceptance is obtained by placing the mirror close to the sample and choosing a large reflection angle. The value of h is constrained by the spatial acceptance of the analyzing monochromator, and the distance between sample and mirror should not be too small. Fig. 3 shows the variation of angular acceptance with angle of incidence for a flat mirror.

For the smallest possible angular spread of the reflected beam the mirror should be bent into a parabolic shape, or, in approximation, an elliptical shape with a large magnification is acceptable (Bukreeva *et al.*, 2004). The surface would be described by an eccentricity very close to 1, or exactly 1 for the parabolic shape. For such mirrors the variation of the reflection angle along the mirror surface can become appreciable. The largest and smallest reflection angles, θ_2 and θ_1, respec-

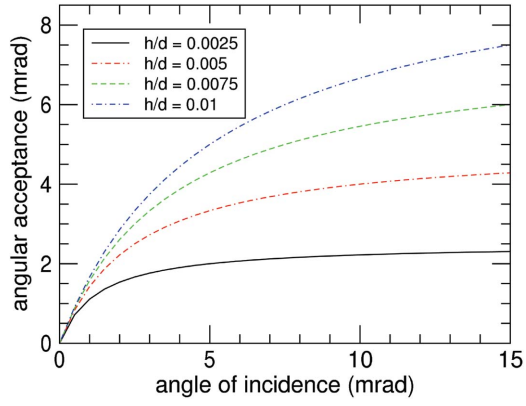

Figure 3
Angular acceptance of a flat mirror *versus* angle of incidence. The value of h/d gives the ratio of reflected-beam height and distance between the mirror's proximal edge and the sample center. The ratio of this distance to the mirror length is assumed to be reasonably large, say larger than 1.

tively, relate the reflecting length L to the distance d between proximal mirror edge and sample by

$$\frac{L}{d} = \left(\frac{\theta_2}{\theta_1}\right)^2 - 1 = 2\frac{\Delta\theta}{\theta_0}\left(1 - \frac{\Delta\theta}{2\theta_0}\right)^{-2}, \quad (1)$$

where $\Delta\theta = \theta_2 - \theta_1$ and $\theta_0 = (\theta_2 + \theta_1)/2$. A derivation of (1) is provided in Appendix *A*. The angular acceptance is given by $\Delta\phi = 2(\theta_2 - \theta_1)$, and the angular spread of the reflected beam is $\Delta\varphi = \Delta\phi(1 - e)/(2\theta_2\theta_1)$, where e is the eccentricity of the mirror ellipse, and the definition of the angles ϕ and φ is apparent in Fig. 10. The magnification factor of the mirror is then given by $M = 2\theta_2\theta_1/(1 - e)$. The height of the reflected beam right after the mirror is given by

$$\frac{h}{L} = \frac{\phi_1\phi_2}{\phi_1 + \phi_2} = \theta_0\left(1 - \frac{\Delta\theta^2}{4\theta_0^2}\right) \quad \text{and} \quad \frac{h}{d} = 2\Delta\theta\frac{\theta_2}{\theta_1}. \quad (2)$$

A derivation of this equation is provided in Appendix *A*. For a Rh metallic coating and 14.4125 keV X-rays the reflectivity stays above 80% for reflection angles less than 4.4 mrad. An angular acceptance of 5 mrad with high reflectivity can be achieved for $\theta_2 = 4.4$ mrad and $\theta_1 = 1.9$ mrad. This results in $L/d = 4.4$ and $h/L = 0.0027$, which means that for reasonable mirror lengths the distance to the sample becomes quite small. An increase of θ_1 provides improvement albeit at the expense of angular acceptance. For $\theta_2 = 4.4$ mrad and $\theta_1 = 2.4$ mrad we obtain a more reasonable $L/d = 2.4$ and $h/L = 0.0031$. With $M > 270$ a mirror of length 20 cm at 8 cm distance from the sample would collect 4 mrad and, for a point source, produce a reflected beam of less than 15 µrad angular spread with a height of 0.62 mm.

Higher angular acceptance could be achieved with a multilayer coating. However, the multilayer periodicity would have to be graded appropriately to account for high reflectivity along the whole length of the mirror surface. The variation of the reflection angle θ along the mirror surface is derived in Appendix *A* and is expressed by

$$\theta = \frac{\theta_1\theta_2}{\left[z\theta_1^2 + (1 - z)\theta_2^2\right]^{1/2}}, \quad (3)$$

where the normalized mirror coordinate $0 \leq z \leq 1$ increases linearly along the surface. At 14.4125 keV, reflectivities above 80% in the first-order multilayer peak are possible. For such a mirror, $\theta_2 = 12$ mrad and $\theta_1 = 7$ mrad would give an angular acceptance of 10 mrad. We also obtain $L/d = 1.9$ and $h/L = 0.0088$. With $M > 670$ a mirror length of 20 cm and a distance 10 cm from the sample would collect 10 mrad and produce a reflected beam of less than 15 µrad angular spread but with a height of 1.76 mm. The high magnification and the large beam height probably pose technical problems that require us to relax the angular acceptance. For example, $\theta_2 = 12$ mrad and $\theta_1 = 8$ mrad would give an angular acceptance of 8 mrad with $L/d = 1.25$ and $h/L = 0.0096$. With $M > 530$ a mirror of length 10 cm at 8 cm distance from the sample would collect 8 mrad and produce a reflected beam of less than 15 µrad angular spread and a height of 0.96 mm. If an even smaller beam height is desired, $\theta_2 = 12$ mrad and $\theta_1 = 9$ mrad would give an angular acceptance of 6 mrad with $L/d = 0.78$ and $h/L = 0.01$. With $M > 400$ a mirror of length 6 cm and distance 8 cm from the sample would collect 6 mrad and, for a point source, produce a reflected beam of less than 15 µrad angular spread and a height of 0.62 mm. The numerical examples are summarized in Table 1. In comparison with uniformly coated mirrors, the advantage of the graded-multilayer mirror is to allow large angular acceptance with short mirrors. However, the large beam height and magnification factors could pose technical problems.

Table 1
Parameters for potential collimating mirrors.

Graded multilayer (ML) coatings allow larger angular acceptances and short mirrors at the expense of large exit beam height. All angle values are given in units of mrad. d: distance between source center and proximal edge of mirror; L: length of mirror; h: height of reflected beam; θ_1: lowest reflection angle; θ_2: highest reflection angle; $\Delta\phi$: angular acceptance; M: magnification factor; $\Delta\varphi$: divergence of reflected beam assuming a point source.

Type	d (cm)	L (cm)	h (mm)	θ_1	θ_2	$\Delta\phi$	M	$\Delta\varphi$
Rh coated	8	35.2	0.95	1.9	4.4	5	333	0.015
Rh coated	8	19.2	0.59	2.4	4.4	4	267	0.015
Graded ML	10	19	1.7	7	12	10	667	0.015
Graded ML	8	10	0.96	8	12	8	533	0.015
Graded ML	8	6.2	0.62	9	12	6	400	0.015
Rh coated	14	61.6	1.66	1.9	4.4	5	10	0.5
Graded ML	14	26.6	2.3	7	12	10	20	0.5

So far we have discussed the collimation of the X-rays in one dimension of angle. The two-dimensional collimation of X-rays is considerably more difficult to achieve with proven technologies. The precise bending of a reflecting surface in two directions is not within reach at present. We therefore have to use either two independently bent reflecting surfaces, such as a Kirkpatrick–Baez arrangement, or just one-dimensional collimation and consider the consequences for the analyzing process. We will now discuss the first option, an elliptically bent mirror orthogonal to the preceeding one.

The minimum distance of this second mirror from the sample is given by the sum of quantities d and L introduced earlier. The smallest values for $L + d$ can be achieved for a graded-multilayer first mirror. A first mirror of length 6 cm and distance 8 cm from the sample would collect 6 mrad and give $d' = L + d = 14$ cm. For a Rh-coated second mirror an angular acceptance of 5 mrad with high reflectivity can then be achieved for $\theta_2 = 4.4$ mrad and $\theta_1 = 1.9$ mrad resulting in $L'/d' = 4.4$ and $h'/L' = 0.0027$. The length of the second mirror therefore would have to be 62 cm with an exit beam height of 1.7 mm. For a graded-multilayer second mirror, $\theta_2 = 12$ mrad and $\theta_1 = 7$ mrad would give an angular acceptance of 10 mrad and $L'/d' = 1.9$ and $h'/L' = 0.0088$ resulting in a length of the second mirror of 27 cm with an exit beam height of 2.3 mm. The magnification factor is less critical for the second than for the first mirror because the angular acceptance of the analyzing monochromator perpendicular to its scattering plane is large. However, as discussed later, a deterioration of energy resolution by approximately $\delta E = E_0\vartheta^2/2$ is expected as a result of angular acceptance 2ϑ. With $\delta E/E_0 < 10^{-7}$ the requirement $2\vartheta < 0.9$ mrad must therefore be met, and the

magnification factor of the second mirror becomes $M \gtrsim 10$. The numerical examples are summarized in Table 1.

Slope errors have the potential to limit the effectiveness of the collimating mirrors. As shown in Appendix *A*, rays leaving the source at angle ϕ will be incident on the mirror surface at angle $\theta = \phi/2$ and approach the image point under an angle of $\varphi = 2(1 - e)/\phi$. Slope errors are deviations from elliptical shape, and, for a source ray of angle ϕ, the incidence angle on the mirror surface will be different from the ideal value of $\phi/2$, *i.e.* $\theta = \phi/2 + \alpha$. The angle γ describes the local distortion of the mirror surface and leads to mis-steered reflected rays which now propagate at angles of $\varphi = 2(1 - e)/\phi + 2\gamma$. This effect will be particularly noticeable for parabolically shaped surfaces for which $e = 1$. If the distortions γ are sufficiently random in their distribution, for example in the perpendicular direction, then it will be reasonable to express the effect of these slope errors as an increase in the angular spread,

$$\Delta\varphi = \left(\Delta\varphi_0^2 + 4\Delta\gamma^2\right)^{1/2}, \tag{4}$$

where $\Delta\varphi_0$ is the angular spread from the undistorted mirror and $\Delta\gamma$ is the r.m.s. slope error. For a collimating mirror in the M^4 instrument the slope errors therefore must be smaller than half the permissible divergence of the X-ray beam on the monochromator, but preferably should be even smaller. For example, if $\Delta\varphi_0 = 15$ µrad, then a slope error of $\gamma = 5$ µrad leads to $\Delta\varphi = 18$ µrad, which may reduce the overall efficiency noticeably.

2.2. Source size effects

The contribution of the source size to the divergence of the collimated X-rays is determined by the transverse dimension of the source, the distance of the reflecting surface to the source, and to some extent by the length of the mirror. The length of the source may also become important as discussed later. If s is the size of the illuminated area of the sample, d is the distance between this area and the proximal edge of the mirror, and L is the length of the mirror, then the source-size-induced divergence is bound by $s/(d + L)$ and s/d, and the average value over the length of the mirror is given by

$$\delta\phi = \frac{s}{L}\ln\left(1 + \frac{L}{d}\right). \tag{5}$$

This contribution is potentially more serious for vertical collimation because of the small angular acceptance of the analyzing monochromator. A large source-size contribution to the divergence of the collimated X-rays would strongly reduce the efficiency of the analyzing process. A limitation of $\delta\phi < 10^{-5}$ leads to $s < L/\ln(1 + L/d) \times 10^{-5}$ and the mirror scenarios discussed earlier give $s < 1.6$ µm for the Rh-coated mirror and $s < 1.1$ µm for the graded-multilayer mirror.

The requirements for a horizontally focusing mirror are more relaxed, but for a high-resolution instrument we still require $\delta\phi < 2 \times 10^{-4}$ leading to $s' < 2L'/\ln(1 + L'/d') \times 10^{-4}$. For the graded-multilayer mirror design proposed earlier, we then require for the horizontal source size $s' < 50$ µm. Therefore it seems practical to operate the M^4 instrument in horizontal geometry, *i.e.* the inelastic scattering plane is perpendicular to the diffraction plane of the analyzing monochromator. Then the horizontal source size, contrary to the vertical source size, is not just determined by the horizontal X-ray beam size incident on the sample but also by the projection of the X-ray beam passing through the sample. The apparent horizontal source size is then estimated by

$$s' = s_0' \cos\alpha + a \sin\alpha \leq \left(a^2 + s_0'^2\right)^{1/2}, \tag{6}$$

where s_0' is the horizontal X-ray beam size incident on the sample, a quantifies the dimension of the scattering source in the direction of the incident beam, and α is the scattering angle. The value of a is mostly related to the absorption length of the X-rays in the sample material. For materials composed of light elements studied at large scattering angles, the apparent source size can quickly exceed the 50 µm quoted earlier for a high-resolution M^4 instrument, and the energy resolution can only be maintained by a reduction in the depth of the sample. In fact, this is a known problem for present-day IXS backreflection instruments as well and potentially reduces the achievable counting rates for light-element compounds.

3. Analyzing monochromator

The critical parameters for the analyzing monochromator are: energy bandwidth; spectral efficiency; vertical angular acceptance; vertical spatial acceptance; horizontal angular acceptance; and, to a lesser extent, horizontal spatial acceptance. For example, the 14.4 keV high-resolution monochromator operating at beamline 3-ID of the Advanced Photon Source has an energy bandwidth of 1.1 meV, spectral efficiency of 25%, vertical angular acceptance of 15 µrad, and a vertical spatial acceptance of 0.7 mm. It uses four flat asymmetrically cut silicon crystals with reflections (4 0 0), (4 0 0), (10 6 4), (10 6 4). With similar design principles four flat asymmetrically cut silicon crystals with all (4 0 0) reflections would result in an energy bandwidth of 10 meV, spectral efficiency of 45%, and vertical angular acceptance of 27 µrad. Further improvement in efficiency is expected with an increase of the energy bandwidth.

The specifications of the collimating mirror assembly largely determine the properties of the X-ray beam incident on the analyzing monochromator. We will assume here that the preceeding mirror has prepared the beam divergence and size in the scattering plane of the monochromator (vertical) to acceptable levels. The remaining discussion in this section will revolve around the consequences of divergence perpendicular to the scattering plane (horizontal). A previous study showed (Bortel *et al.*, 2000) that the transmitted energy E for rays having an angle ϑ out of the principal diffraction plane is given by

$$E = \frac{E_0}{\cos\vartheta} \simeq E_0 + \frac{E_0}{2}\vartheta^2. \tag{7}$$

For an analyzer operating at 14.4 keV accepting 10 mrad horizontally, the energy shift becomes $E - E_0 = 180$ meV for the extremal rays, and this is much too large for a high-reso-

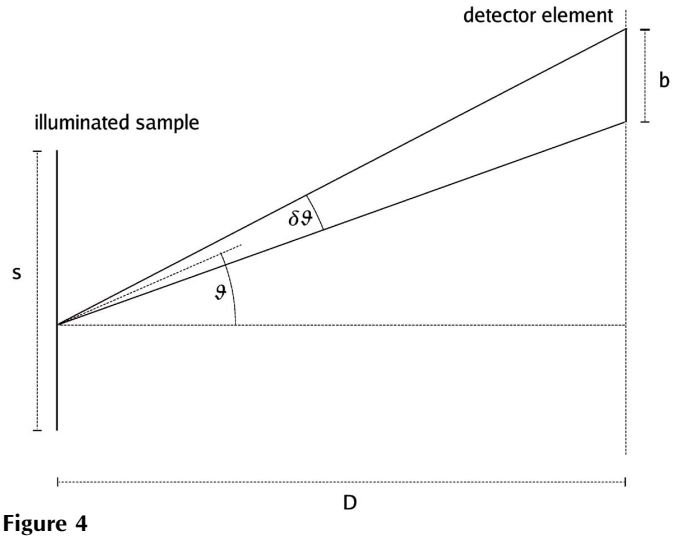

Figure 4
Schematic of the geometric relations between illuminated sample region and a detector element. The analyzing monochromator and collimating mirrors located between sample and detector are not shown.

lution instrument. A possible solution to avoid associated energy broadenings is the use of a horizontally collimating mirror as discussed in the previous section. At 14.4 keV a horizontal divergence of 0.65 mrad would cause an extremal shift of 3 meV and an average broadening owing to different shifts at different angles of about 1 meV. However, the known correlation between angle and energy expressed by (7) could be utilized to recover the energy resolution with a position-sensitive detector following the analyzing monochromator. Fig. 4 shows the important geometric relations, and some examples are summarized in Table 2. In practice, the energy resolution somewhat deteriorates as a result of the combined size of the illuminated sample area and detector size which causes an angular spread estimated by $\delta\vartheta < (b + s)/D$, where s is the characteristic size of the illuminated sample area. Using (7) the angular spread leads to an energy spread $\delta E = E_0\vartheta\delta\vartheta$ which combines with the intrinsic energy bandwidth of the analyzing monochromator δE_i to give an effective analyzer bandwidth of $\delta E_\mathrm{a} = (\delta E^2 + \delta E_\mathrm{i}^2)^{1/2}$. If we specify intrinsic and effective bandwidths, operating energy, and detector–sample distance the following constraint for the sum of sample source size and detector-element size is obtained,

$$b + s < D\frac{\left(\delta E_\mathrm{a}^2 - \delta E_\mathrm{i}^2\right)^{1/2}}{E_0}\frac{1}{\vartheta}. \qquad (8)$$

For 14.4 keV operating energy, intrinsic bandwidth of 1 meV, effective bandwidth of 1.5 meV, horizontal deflection of 5 mrad, and a sample–detector distance of 2 m, this results in $b + s < 31$ µm. At present, focusing routinely achieves $s < 20$ µm and 10 µm seems reasonable. The size of a detector element therefore has to be smaller than 20 µm for 2 m distance from the sample. We can also write $(b + s)/D < 7.8 \times 10^{-8}/\vartheta$ and notice that the size of a detector element becomes more critical for larger deflection angles. A fixed value for $b + s$ creates a constraint on distance and deflection $D/\vartheta > 1.3(b + s) \times 10^7$. A position-sensitive detector with N elements of size b covers an angular deflection of $\vartheta = bN/(2D)$. In combination with previous bandwidth requirements, this detector can operate at a deflection angle of at most $\vartheta_\mathrm{max} = 2 \times 10^{-4}[Nb/(b + s)]^{1/2}$ with a corresponding distance $D = 2.6 \times 10^3[Nb(b + s)]^{1/2}$. A present-day strip detector offers pixel sizes of 50 µm × 200 µm with 256 elements. Such a detector could accommodate deflection angles of at most 2.8 mrad, equivalent to a horizontal acceptance of 5.6 mrad, and would have to be placed at a distance of 2.3 m from the sample. A gain of angular acceptance requires larger deflection angles ϑ which according to (8) requires a proportionate decrease in pixel size or increase in distance. But the actual size of the detector would also have to increase in proportion to capture the larger X-ray beam. Assuming the same size for each pixel, both effects combine for a quadratic dependence of number of pixels with angular acceptance.

Table 2
Parameters for potential position-sensitive detectors.

s: apparent horizontal source size; b: size of detector element; D: distance between source and detector; 2ϑ: horizontal angular acceptance; δE: energy broadening; $E - E_0$: energy range; N: number of detector elements.

s (µm)	b (µm)	D (m)	ϑ (mrad)	δE (meV)	$E - E_0$ (meV)	N
10	20	2	5	1	180	1000
10	50	4	5	1	180	800
10	50	2.3	2.8	1	57.6	256
50	50	2.6	1.92	1	26.5	256
50	50	0.82	6.1	10	268	256
100	50	5	33	10	8000	2222

For M^4 instruments designed for smaller energy resolution, the use of a position-sensitive detector is more attractive. For example, an operating energy of 14.4 keV, intrinsic bandwidth of 10 meV, effective bandwidth of 15 meV, horizontal deflection of 5 mrad, and a sample–detector distance of 2 m results in $b + s < 310$ µm. With focusing, the size of a detector element therefore has to be smaller than 300 µm for 2 m distance from the sample, and thus $(b + s)/D < 7.8 \times 10^{-7}/\vartheta$. The maximum deflection angle now becomes $\vartheta_\mathrm{max} = 6.3 \times 10^{-4}[Nb/(b + s)]^{1/2}$. The same strip detector now accepts 18.3 mrad horizontally and has to be positioned at a distance of 0.72 m from the sample. In conclusion, we find that a high-resolution instrument ($\Delta E \simeq 1$ meV) requires vertical and horizontal collimation of the inelastically scattered radiation, whereas a medium-resolution analyzer ($\Delta E \gtrsim 10$ meV) only needs vertical collimation if used in combination with a position-sensitive detector.

4. Ray-tracing calculations

We used the *SHADOW* ray-tracing code to simulate several scenarios of the collimating mirrors of an M^4 instrument. All simulations were performed for an operating energy of 14.4 keV. Our earlier estimates showed that graded-multilayer mirrors outperform single-layer mirrors in terms of angular acceptance. The simulated mirror arrangement using two graded-multilayer mirrors is shown in Fig. 5. The angle of incidence in the center of each mirror was 10 mrad. In

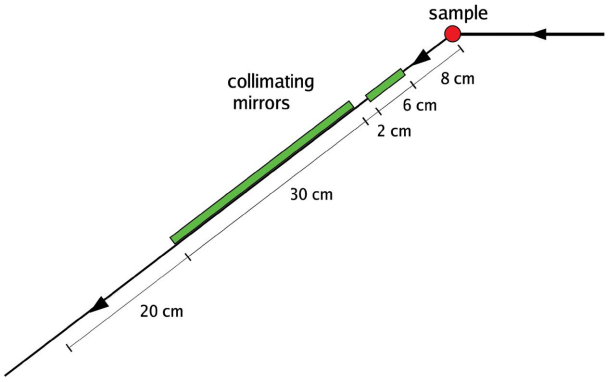

Figure 5
Mirror arrangement for ray-tracing calculations. The scattering volume of the focused X-ray beam on the sample defines the source. A location 20 cm past the end of the second mirror defines the exit beam.

different simulations we varied the vertical and the apparent horizontal source size and analyzed the divergence and size of the exit beam. The vertical and horizontal angular acceptances are 5.74 mrad and 10.6 mrad, respectively. The height and width of the exit beam are 0.59 mm and 2.9 mm, respectively. They are basically unaffected by the source size.

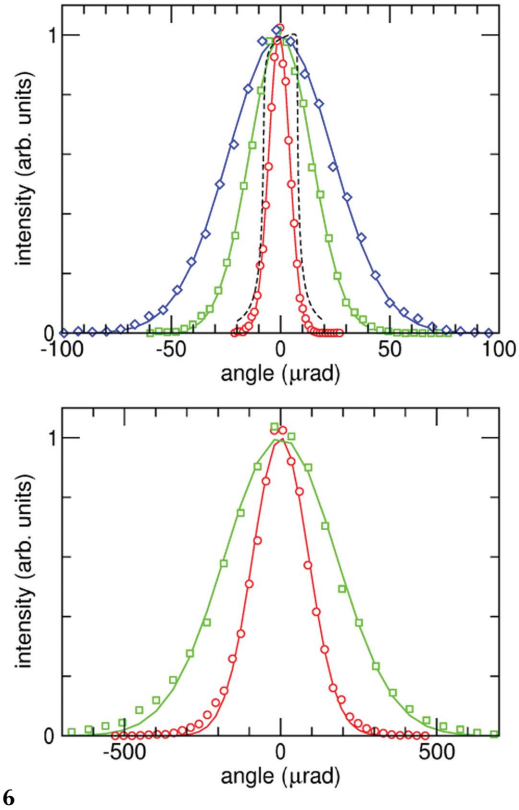

Figure 6
Vertical and horizontal divergence of the exit beam. Top panel: symbols show ray-tracing results for vertical source sizes of 1 μm (circles), 3 μm (squares) and 5 μm (diamonds). The solid lines are Gaussian fits with vertical FWHM widths of 11.2 μrad, 33.5 μrad and 56 μrad. The dashed line is the angular acceptance of the 14.4 keV 1 meV-resolution monochromator operating at 3-ID. Bottom panel: symbols show ray-tracing results for horizontal source sizes of 50 μm (circles) and 100 μm (squares). The solid lines are Gaussian fits with horizontal FWHM widths of 210 μrad and 420 μrad.

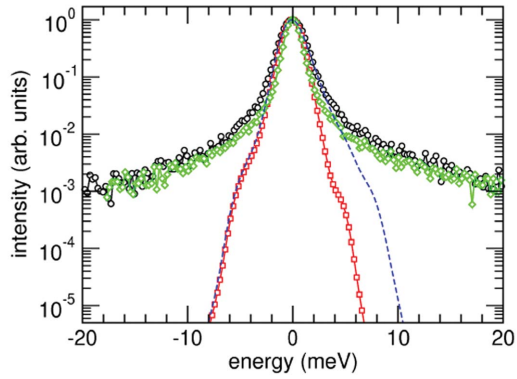

Figure 7
Influence of horizontal source size on energy resolution function. Black circles: APS 3-ID, 2.2 meV FWHM, 21.6 keV. Green diamonds: APS 30-ID, 1.5 meV FWHM, 23.7 keV. Both instruments feature backreflection analyzers. Red squares: M^4 instrument calculated as a self-convolution of the measured resolution function of the in-line monochromator operating at APS 3-ID, 1.6 meV FWHM, 14.4 keV. The blue dashed line shows the effect of a 100 μm horizontal source size.

The vertical divergence of the exit beam is mostly sensitive to the vertical size of the focused X-rays on the sample. In Fig. 6 the vertical divergence is shown to be between 11.2 μrad and 56 μrad for focus spots between 1 μm and 5 μm, respectively, and will affect the efficiency of the analyzer.

The horizontal divergence is 210 μrad and 420 μrad for focus spots of 50 μm and 100 μm, respectively. According to (7) the horizontal divergence potentially worsens the energy resolution of the instrument. We therefore calculated the energy spread and convoluted the result with the M^4 instrument resolution function shown in Fig. 2. A horizontal source of 50 μm has no discernible effect on the resolution function. However, a 100 μm source size shows some broadening toward positive energy values as shown in Fig. 7. It is important to note that the shape of the horizontal source matters. In particular, extended wings in the focal spot should be avoided.

Bending of the mirror leads to a variation of incidence angles along the surface as described by (3). The results of the ray-tracing calculations are shown in Fig. 8. Besides the mirror length L and source distance d, the incidence angle in the mirror center θ_i was an input parameter. These parameters relate to $\theta_{1,2}$ in (3) by

$$\theta_1 = \theta_i\left[\frac{2d+L}{2(d+L)}\right]^{1/2} \quad \text{and} \quad \theta_2 = \theta_i\left(1+\frac{L}{2d}\right)^{1/2}. \qquad (9)$$

For vertical and horizontal mirrors we then obtain θ_1 = 8.863 mrad, θ_2 = 11.72 mrad and θ_1 = 8.21 mrad, θ_2 = 13.92 mrad, respectively. With these values the ray-tracing results are well described by (3), but, in addition, we observe a distribution of angles for each position along the mirror. These distributions are source size effects and may reduce the average mirror reflectivity. For an energy of 14.4 keV we calculated the reflectivity of a Rh/Si multilayer with 70 periods and individual layer thicknesses of 3 nm to 1.7 nm, which correspond to reflection peak positions of 8 mrad and 13.9 mrad, respectively. The widths of the peaks are about 0.7 mrad and 0.43 mrad and are larger than the distribution of

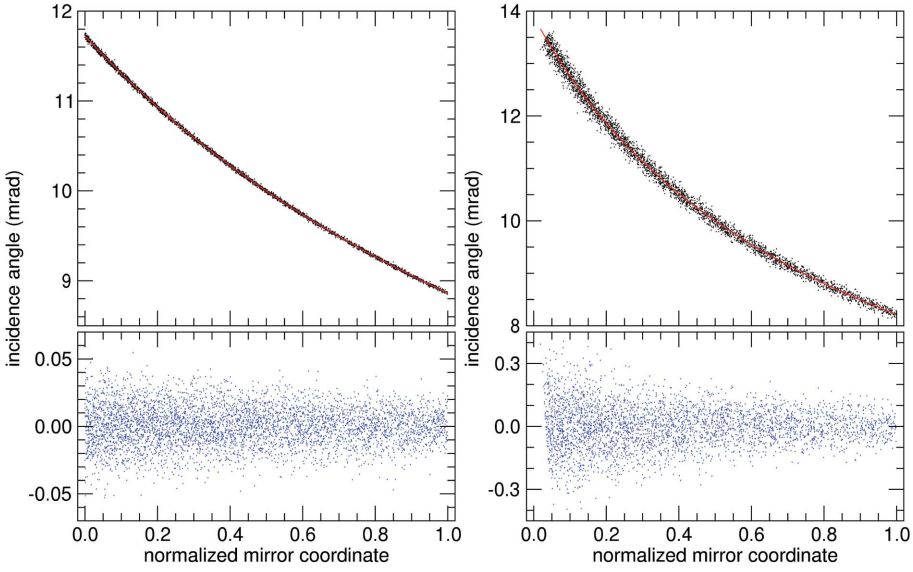

Figure 8
Variation of incidence angles along vertical (left) and horizontal (right) mirror surfaces. The red lines are calculated using (3) as explained in the text. The graphs at the bottom illustrate the angular distributions around the calculated curves which are a result of finite source sizes of 3 μm vertically and 50 μm horizontally.

incidence angles. The situation is illustrated in Fig. 9. For a mirror with appropriate lateral grading we therefore expect a reflectivity of at least 80%. A recent study by Honnicke *et al.* (2010) discusses the important design issues for collimating graded-multilayer mirrors in detail.

The ray-tracing results using vertical and horizontal source sizes of 1 μm and 50 μm, respectively, combine to give an analyzer performance of 6.1×10^{-5} sterad angular acceptance and 16% efficiency if we assume 80% reflectivity per collimating mirror and an efficiency of 25% for the monochromator. These values compare with 2.2×10^{-4} sterad angular acceptance and 13% efficiency for a single backreflection analyzer for the IXS instrument at 3-ID of the APS operating at 21.6 keV. The analyzer of a 14.4 keV M^4 instrument therefore performs at 34% of an existing IXS instrument. However, this performance is achieved at a lower operating energy. The intensity of the X-ray source and potential absorption losses in beamline components, transfer lines and sample environments need to supplement the given numbers. If we factor all components the in-line analyzer of a high-resolution 14.4 keV M^4 instrument could perform similarly to a single backscattering analyzer of existing IXS instruments.

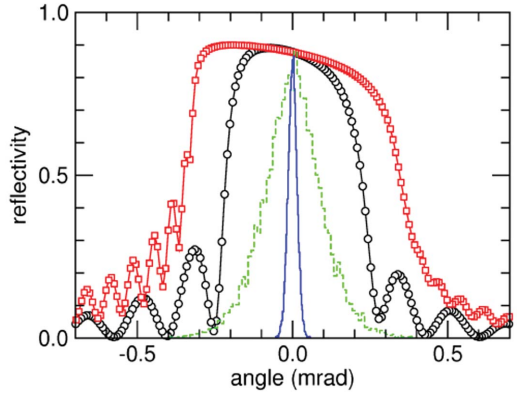

Figure 9
Multilayer reflectivity and distribution of incidence angles for vertical and horizontal mirror surfaces. Red squares: multilayer peak at 8 mrad for a Rh/Si multilayer with 70 periods and layer thicknesses of 3 nm. Black circles: multilayer peak at 13.9 mrad for a Rh/Si multilayer with 70 periods and layer thicknesses of 1.7 nm. Blue solid line: histogram of incidence angles for vertical mirror. Green dashed line: histogram of incidence angles for horizontal mirror. The histograms were generated from the angular distributions shown in the bottom panels of Fig. 8. The multilayer peaks are shifted to allow proper comparison.

Based on the previous performance numbers we expect a significant improvement in sensitivity for a 15 meV resolution M^4 instrument using 10 meV monochromators as described earlier. Removal of the horizontally collimating mirror and bandwidth-efficiency increase combine to enhance sensitivity by a factor of about 400. However, it should be mentioned that the requirement to focus the X-rays incident on the sample to only a few micrometers will impact the overall efficiency of an M^4 instrument.

The horizontal angular acceptance leads to a momentum resolution of this M^4 analyzer of 0.77 nm^{-1} which compares favorably with the 1.63 nm^{-1} momentum resolution of the backreflection analyzer at 3-ID of the APS. These values have to be compounded with the divergence of the X-rays that are incident on the sample. The focusing mirror can significantly increase this value over the divergence of the synchrotron radiation source. Third-generation synchrotron source sizes and divergences are typically (vertical times horizontal) 20 μm × 500 μm and 15 μrad × 35 μrad, respectively. The need for a 1 μm × 20 μm focus would then increase the divergence at the sample to 0.3 mrad × 0.875 mrad. However, the analyzer acceptance of 5.74 mrad × 10.6 mrad remains the dominating contribution to the overall momentum resolution of the M^4 instrument.

5. Summary

In this paper we demonstrated that an M^4 instrument would be comparable in performance with existing IXS instruments. The design challenges lie in the vertical focal spot size on the sample, the production of laterally graded multi-layer mirrors, and the implementation of an analyzing monochromator with large angular acceptance. The optimization of an M^4 instrument is less demanding if the energy resolution is relaxed or the operating energy is lowered. Energy resolutions of 10–100 meV and lower operating energies would permit more efficient in-line monochromators with larger angular acceptance to be employed. Lower operating energies also allow larger angular acceptances of the collimating mirrors. In

practice, however, lower operating energies typically increase X-ray absorption losses in sample and sample environments, such as containers or high-pressure devices. In addition, the intensity and brilliance of the synchrotron source needs to be considered for global optimization of the M^4 instrument. The superior energy resolution function of the M^4 instrument in combination with independent choice of operating energy and energy resolution would provide ample scientific opportunities.

APPENDIX *A*
Derivations of equations (1), (2) and (3)

The surface of an elliptical mirror constitues part of an ellipse as shown in Fig. 10. As is well known, $\rho + \eta = 2a$, and the location of all points on the ellipse is described by

$$\eta(\phi) = a\frac{1-e^2}{1-e\cos\phi}. \tag{10}$$

The incidence angle θ at the mirror surface was calculated as (Bukreeva *et al.*, 2004)

$$\theta(\phi) = \left|\arctan\frac{1-e\cos\phi}{e\sin\phi}\right|. \tag{11}$$

For grazing-incidence optics the eccentricity is very close to 1, *i.e.* $e = 1-\varepsilon$ and $\varepsilon \ll 1$. Also the angles ϕ, θ and φ are very small, typically of the order of several microradians. Under these conditions we obtain

$$\eta(\phi) = a\frac{4\varepsilon}{\phi^2+2\varepsilon} \qquad \text{and} \qquad \theta(\phi) = \frac{\phi}{2}+\frac{\varepsilon}{\phi}. \tag{12}$$

The generally valid relationship $\phi + \varphi = 2\theta$ then also implies that $\phi\varphi = 2\varepsilon$ and thus $\theta = \phi/2$ is justified. The collimation strength of the mirror could be described by $F = |\mathrm{d}\phi/\mathrm{d}\varphi|$ resulting in $2\varepsilon = \phi^2/F$. For the strongly collimating mirrors discussed in this paper the value of ε is therefore considerably smaller than ϕ^2, and it is justified to simplify (12) further by using $\eta(\phi) = 4a\varepsilon/\phi^2$ and $\theta = \phi/2$.

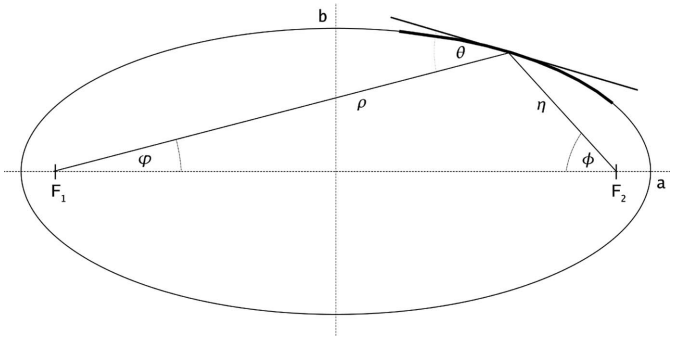

Figure 10
Elliptical mirror geometry. The lengths of the axes of the ellipse are $2a$ and $2b$, and the eccentricity is defined as $e = (1-b^2/a^2)^{1/2}$. Rays propagate from the source located at focal point F_2, are reflected at the mirror surface, and create an image at focal point F_1. For grazing-incidence optics the eccentricity is very close to 1, and the angles ϕ, θ and φ are very small.

The reflecting mirror length is obtained by integration along the ellipse between angles ϕ_2 and ϕ_1 corresponding to the near and far edge of the mirror as seen from source point F_2,

$$L = \int_{\phi_1}^{\phi_2}\left[\eta^2+\left(\frac{\partial\eta}{\partial\phi}\right)^2\right]^{1/2}\mathrm{d}\phi$$
$$= 8a\varepsilon\int_{\phi_1}^{\phi_2}\frac{\mathrm{d}\phi}{\phi^3} = 4a\varepsilon\left(\frac{1}{\phi_1^2}-\frac{1}{\phi_2^2}\right), \tag{13}$$

where in the second line we used the grazing-incidence approximations and assumed strong collimation, *i.e.* $F \gg 1$. The result of the integration in combination with the expression for the near-edge distance to the source, $d = \eta(\phi_2) = 4a\varepsilon/\phi_2^2$, leads to

$$\frac{L}{d} = \frac{\phi_2^2-\phi_1^2}{\phi_1^2}, \tag{14}$$

and, with $\phi = 2\theta$, equation (1) is obtained.

For a strongly collimating mirror the angle φ will be very small and reflected rays will be almost parallel to the baseline of the ellipse drawing in Fig. 10. The exit-beam height is calculated as the difference between the above baseline positions of the rays reflected off the proximal and distal mirror edge, respectively. Those positions are $y_1 = \eta(\phi_1)\sin\phi_1$ and $y_2 = \eta(\phi_2)\sin\phi_2$. With previous assumptions of grazing-incidence conditions we obtain

$$h = y_1 - y_2 = 4a\varepsilon\left(\frac{1}{\phi_1}-\frac{1}{\phi_2}\right). \tag{15}$$

This equation in combination with (13) gives (2).

The variation of the incidence angle along the mirror surface can be obtained from (13) with $\phi = 2\theta$,

$$L(\theta) = a\varepsilon\left(\frac{1}{\theta_1^2}-\frac{1}{\theta^2}\right), \tag{16}$$

where $\theta_1 \le \theta \le \theta_2$ and $L(\theta_1) = 0$. After introducing a normalized mirror coordinate $z = L(\theta)/L(\theta_2)$ and solving the previous equation for θ we directly obtain (3).

We thank Drs E. E. Alp and A. Alatas for discussions aiding the preparation of the paper. This work was supported by the US Department of Energy, Office of Science, Office of Basic Energy Sciences, under Contract No. DE-AC02-06CH11357.

References

Baron, A. Q. R., Tanaka, Y., Ishikawa, D., Miwa, D., Yabashi, M. & Ishikawa, T. (2001). *J. Synchrotron Rad.* **8**, 1127–1130.
Bortel, G., Alp, E. E., Sturhahn, W. & Toellner, T. S. (2000). *J. Synchrotron Rad.* **7**, 333–339.
Bukreeva, I. N., Dabagov, S. B. & Lagomarsino, S. (2004). *Appl. Opt.* **43**, 6270–6277.
Burkel, E. (2000). *Rep. Prog. Phys.* **63**, 171.

Chumakov, A. I., Metge, J., Baron, A. Q. R., Grünsteudel, H., Grünsteudel, H. F., Rüffer, R. & Ishikawa, T. (1996). *Nucl. Instrum. Methods Phys. Res. A*, **383**, 642–644.
Chumakov, A. I., Rüffer, R., Leupold, O., Barla, A., Thiess, H., Asthalter, T., Doyle, B. P., Snigirev, A. & Baron, A. Q. R. (2000). *Appl. Phys. Lett.* **77**, 31–33.
Honnicke, M. G., Huang, X., Keister, J. W., Kodituwakku, C. N. & Cai, Y. Q. (2010). *J. Synchrotron Rad.* **17**, 352–359.
Hu, M. Y., Toellner, T. S., Sturhahn, W., Hession, P., Sutter, J. & Alp, E. E. (1999). *Nucl. Instrum. Methods Phys. Res. A*, **430**, 271–276.
Krisch, M. & Sette, F. (2007). *Inelastic X-ray Scattering from Phonons, Light Scattering in Solids*, pp. 317–370. Berlin: Springer Verlag.
Mooney, T. M., Toellner, T. S., Sturhahn, W., Alp, E. E. & Shastri, S. D. (1994). *Nucl. Instrum. Methods Phys. Res. A*, **347**, 348–351.
Shvydko, Y. (2004). *X-ray Optics: High-Energy-Resolution Applications, Springer Series in Optical Sciences.* Berlin: Springer.
Sinn, H., Alp, E. E., Alatas, A., Barraza, J., Bortel, G., Burkel, E., Shu, D., Sturhahn, W., Sutter, J., Toellner, T. & Zhao, J. (2001). *Nucl. Instrum. Methods Phys. Res. A*, **467–468**, 1545–1548.
Sutter, J. P., Baron, A. Q. R., Miwa, D., Nishino, Y., Tamasaku, K. & Ishikawa, T. (2006). *J. Synchrotron Rad.* **13**, 278–280.
Toellner, T. S. (2000). *Hyperfine Interact.* **125**, 3–28.
Toellner, T. S., Alatas, A., Said, A., Shu, D., Sturhahn, W. & Zhao, J. (2006*a*). *J. Synchrotron Rad.* **13**, 211–215.
Toellner, T. S., Hu, M. Y., Bortel, G., Sturhahn, W. & Shu, D. (2006*b*). *Nucl. Instrum. Methods Phys. Res. A*, **557**, 670–675.
Toellner, T. S., Hu, M. Y., Sturhahn, W., Bortel, G., Alp, E. E. & Zhao, J. (2001). *J. Synchrotron Rad.* **8**, 1082–1086.
Toellner, T. S., Hu, M. Y., Sturhahn, W., Quast, K. W. & Alp, E. E. (1997). *Appl. Phys. Lett.* **71**, 2112.
Yabashi, M., Tamasaku, K., Kikuta, S. & Ishikawa, T. (2001). *Rev. Sci. Instrum.* **72**, 4080–4083.
Yavas, H., Alp, E. E., Sinn, H., Alatas, A., Said, A. H., Shvyd'ko, Y., Toellner, T., Khachatryan, R., Billinge, S. J. L., Hasan, M. Z. & Sturhahn, W. (2007). *Nucl. Instrum. Methods Phys. Res. A*, **582**, 149–151.
Zhao, J. Y., Toellner, T. S., Hu, M. Y., Sturhahn, W., Alp, E. E., Shen, G. Y. & Mao, H.-K. (2002). *Rev. Sci. Instrum.* **73**, 1608.